JOURNAL OF SPACECRAFT AND ROCKETS
Vol. 47, No. 5, September–October 2010

Modeling of Sodium Radiation from Reentry Flows at High Altitudes

Jiaqiang Zhong* and Deborah A. Levin†
Pennsylvania State University, University Park, Pennsylvania 16802

DOI: 10.2514/1.40441

A kinetic-based quasi-steady-state model is developed to study sodium radiation intensity for reentry high-altitude flows of the blunt-body Stardust and a slender body. The sodium detected in the high-speed Stardust-reentry flow was from an impurity of the ablative thermal protection material. In this work, the particle-based direct simulation Monte Carlo method is used to obtain flow solutions, and a quasi-steady-state model is used to derive the sodium number-density distributions in the ground and excited electronic states. The sodium radiation intensity is calculated based on the sodium number-density distributions in the excited states and agrees reasonably well with the observation data for the Stardust reentry at 81 km. It was also found that sodium radiation in the slender-body reentry flow will be orders of magnitude less than the value observed for the blunt body.

Nomenclature

A	=	coefficient, surface area
B	=	coefficient
c	=	light speed
d	=	distance
E	=	energy
e^-	=	electron
h	=	Planck constant
I	=	radiation intensity
k	=	reaction rate, Boltzmann's constant
M	=	neutral species
m	=	molecular mass
N	=	number density
Na	=	sodium atom
T	=	temperature
t	=	time
x	=	distance along a line of sight
λ	=	wave length
σ	=	cross section
τ	=	lifetime of excited state

Subscripts

a	=	atomic species
e	=	electron species
g	=	ground state
i	=	atomic ground or excited state
1	=	first excited state
2	=	second excited state

I. Introduction

THE analysis of spectra data provides an important metric for quantitatively evaluating the performance of high-speed reentry vehicles, where flows are characterized as nonequilibrium and chemical reacting. Most of the available reentry radiation studies have been focused on emissions from air species. For example, Dong et. al. [1] recently developed a multitemperature coupled vibration dissociation model to calculate air-species radiation in a shock tube. Wray et. al. [2] applied multiband methods based on the use of the opacity distribution function to calculate Apollo reentry flow air radiation. However, it is important to understand the radiation emitted by trace species, such as sodium, because for remote detection with poor spatial resolution, the source of the radiation can clearly be identified with the vehicle. Sodium radiation was detected during a Trailblazer reentry case, as the salt impregnated foam used to protect the spherical rocket motor was exposed to the airstream after the aluminum case was burned through by aerodynamic heating [3]. Lenard [4] applied an approximate method to predict the sodium spatial distribution due to ablative material impurities entering in the boundary region of a hypersonic slender-body reentry flow. Most recently, Jenniskens [5] measured the Stardust-reentry spectra in the wavelength range from 370 to 880 nm using a slitless Echelle spectrograph, and the sodium-excitation spectra was observed.

Since the sodium in the Stardust entry flow is only from an impurity of the ablative thermal protection system (TPS) material, the interpretation of this spectral feature is potentially simpler than other spectral features in the Echelle spectrographic data. The latter are more complex to model because they involve modeling the spatial distribution of a complex, chemically reacting, nonequilibrium flow. To predict TPS performance, in general, we need to validate our thermochemical nonequilibrium gas dynamic models. As a step in that direction, obtaining good agreement between modeled and measured sodium intensity provides an assessment of the ability to model the electron temperature and electron and neutral concentrations in the flow. In this way, a predictive model of sodium radiation could be important for testing the performance of in-flight reentry space capsules that use ablative TPS material. The purpose of this work is to develop a kinetic-based quasi-steady-state (QSS) model to predict sodium radiation intensity for the Stardust-reentry vehicle by comparison with the measured data. The calibrated model will then be used to predict the sodium intensity that would be observed from a reentry body of a different slender-body shape. We will show that from the remote-sensing aspect, the sodium intensity may provide information about vehicle shape.

In our recent work we have studied high-altitude and transitional-to-continuum reentry flows of the Stardust cometary sample-return capsule in terms of developing new excitation models appropriate to direct simulation Monte Carlo (DSMC) [6] as well as modeling the importance of thermal and chemical ablation [7]. In the first work we studied the change of the flowfield between the altitudes of 100 to 70 km and showed that ultra-high-Mach-number reentry vehicles create sufficiently energetic flow conditions with substantial degrees of ionization, of 1 to 11%, in the noncontinuum flow regime. To

Received 15 August 2008; revision received 2 October 2009; accepted for publication 2 October 2009.

*Postdoctoral Research Fellow, Department of Aerospace Engineering. Member AIAA.

†Professor, Department of Aerospace Engineering. Associate Fellow AIAA.

model these transitional, ionized, and thermochemically nonequilibrium flows, a DSMC approach was investigated and energy-exchange models that have been developed for Navier–Stokes computational fluid dynamics computations were examined and revised for application to the DSMC method. Building on this work, the importance of the ablation processes of the Stardust thermal protection layer on the flowfield and surface parameters was investigated using the DSMC method to model surface thermal and chemical ablation processes as well as ionization processes [7]. It was found that chemical ablation due to reactions between solid carbon and gaseous oxygen and nitrogen atoms is dominant over thermal ablation for the early portion of the reentry. As the altitude decreases, the forebody surface temperature increases, the ablation process becomes more intensive, and the influence of ionization reactions becomes more important due to a denser freestream condition.

In this work, we use the models that were developed in these two earlier papers to study a spectroscopic feature observed in the Stardust-reentry flow Echelle spectral data of Jennenkins [5], as well as a slender-body reentry vehicle at high altitudes [8]. Boyd et al. [9] recently used continuum-based computational fluid dynamics and kinetic-based DSMC solutions as input to the nonequilibrium radiation code, NEQAIR, to compute Stardust-reentry air-species radiation. An interesting aspect of the Echelle data is the strong sodium emission line, as shown in Fig. 1. This figure shows the radiation from the sodium doublet of $^2P_{3/2,1/2}$, which is due to the outgassing or thermal ablation of sodium from the Stardust TPS phenolic impregnated carbon ablator (PICA) material. Laboratory reports[‡] showed that for two unflown samples of PICA studied in inductively coupled plasma ground-based testing, 168 to 308 ppm of sodium have been observed. Sodium radiation has been observed from numerous hypersonic flights and is virtually impossible to quench [3]. Since sodium does not exist in appreciate quantities in the mesospheric portion of the atmosphere, the modeling of this radiation may only be due to outgassing from the TPS material.

To simulate sodium radiation from Stardust, a kinetic-based QSS model is proposed in this work, since there are not sufficient collisions to populate the sodium electronic states in a Boltzmann distribution. The QSS model includes the populations of the sodium ground state as well as the first two electronically excited states of $^2P_{1/2}$ and $^2D_{5/2,3/2}$. Comparison of the predicted radiation with that observed, although spatially averaged over the entire vehicle, provides confirmation of the modeling of the hypersonic boundary layer and its interaction with a charring ablator thermal protection material. As used in previous work [10], an overlay approach wherein the electronically-excited-state species populations are computed based on a converged gas dynamic from the DSMC solution will be employed. This approach is valid in the free-molecular to near-continuum flight regime, because the fraction of sodium is sufficiently low as to not affect the flowfield solution.

This paper is organized as follows. A kinetic-based QSS model for calculation of excited sodium state populations is formulated in Sec. II. Electron- and neutral-impact sodium-ionization cross sections partially required for the QSS model are discussed in Sec. III. Because of low reaction probabilities and high activation energy, it is concluded that the sodium-ionization reactions have negligible impact on the sodium radiation for the cases discussed in this work. In Sec. IV, the developed QSS model is used to calculate the sodium radiation intensity for the blunt-body Stardust and the slender-body 10 deg half-angle-cone reentry flows at high altitudes. Based on excited-state number density and lifetime, the radiation intensity from an excited state to the ground state is integrated over all observation lines. Conclusions are summarized in Sec. V.

II. Kinetic Model for Excited Sodium State Populations

Extensive experimental studies of excited atomic-sodium cross sections exist for many of the important excitation processes and are

[‡]Private communication with M. Stackpoole, 2007.

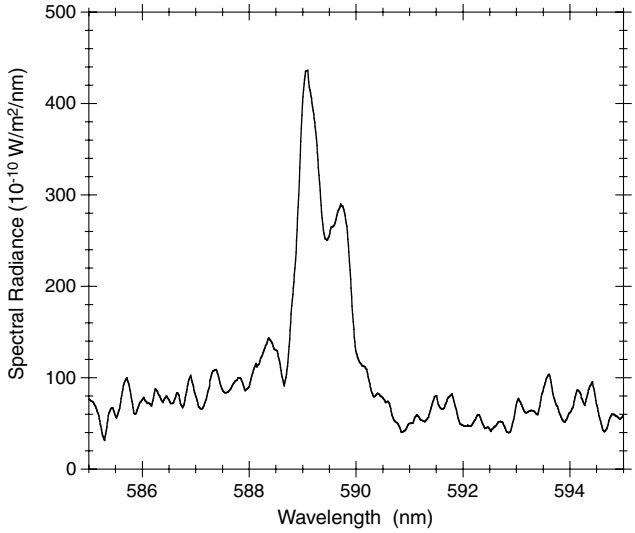

Fig. 1 Echelle spectra of Stardust reentry at approximately 80 km altitude [5].

discussed, for example, in Zecca et al. [11]. The ground-state atomic sodium can be excited to the higher energy levels of $^2P_{1/2}$ $(16,964\ \text{cm}^{-1})$ and $^2D_{5/2}$ $(29,172.8\ \text{cm}^{-1})$ with radiative lifetimes of about 16.4 and 20.0 ns, respectively [12]. The following collisionally induced excitation processes are considered because they potentially impact the number-density distributions of the sodium ground and excitation states [13]:

$$e^- + \text{Na}(g) \rightarrow e^- + \text{Na}(1) \tag{1}$$

$$e^- + \text{Na}(1) \rightarrow e^- + \text{Na}(g) \tag{2}$$

$$e^- + \text{Na}(1) \rightarrow e^- + \text{Na}(2) \tag{3}$$

$$e^- + \text{Na}(2) \rightarrow e^- + \text{Na}(1) \tag{4}$$

$$M + \text{Na}(1) \rightarrow M + \text{Na}(g) \tag{5}$$

$$M + \text{Na}(g) \rightarrow M + \text{Na}(1) \tag{6}$$

$$M + \text{Na}(2) \rightarrow M + \text{Na}(1) \tag{7}$$

$$M + \text{Na}(1) \rightarrow M + \text{Na}(2) \tag{8}$$

$$\text{Na}\,(1) \rightarrow \text{Na}(g) + h\nu_1 \tag{9}$$

$$\text{Na}\,(2) \rightarrow \text{Na}(1) + h\nu_2 \tag{10}$$

The symbol M represents all neutral species (except sodium), and the symbol i can have a value of g, 1, and 2, representing the sodium ground or excited states of $^2P_{1/2}$ and $^2D_{5/2}$, respectively. The rate coefficient values and expressions [14–17] that will be used in the QSS model are given in Table 1. Note that the electron and translational temperatures derived from the DSMC calculations are used in evaluating the rate coefficients given in Eqs. (1–4) and Eqs. (5–8), respectively.

Based on a simple hard-sphere model, the forward reaction rate as a function of reaction collision cross section can be expressed as [18]

$$k_f = \frac{\sigma_R}{\epsilon}\left(\frac{8kT}{\pi m_r}\right)^{0.5}\exp\left(-\frac{E_a}{kT}\right) \tag{11}$$

Table 1 Processes and expressions for rate coefficients and cross sections used in the QSS model for sodium ablation

Excitation Process	Expression	Reference
Electron-impact excitation cross section: (1)–(4)	$\sigma_r = 1.0 \times 10^{-20}$ m^2	[14]
Electron-impact ionization cross section:	$\sigma_r = 1.0 \times 10^{-22}$ m^2	[15,16]
Molecule impact excitation: (5)–(8)	$\sigma_r = 3.0 \times 10^{-19}$ m^2	[17]

where ϵ is a symmetric factor that is equal to unity for reactions (1–8). The last two processes (9) and (10) represent spontaneous emission with a reaction rate of

$$k_f = \frac{1}{\tau} \tag{12}$$

where τ is the lifetime of the excited state.

Using Eqs. (1–10) and Table 1, the time-dependent change of sodium excited state $^2P_{1/2}$ and $^2D_{5/2}$ atomic concentration may be expressed as

$$\frac{\mathrm{d[Na(1)]}}{\mathrm{d}t} = A_g[\mathrm{Na}(g)] - A_1[\mathrm{Na(1)}] + A_2[\mathrm{Na(2)}] \tag{13}$$

$$\frac{\mathrm{d[Na(2)]}}{\mathrm{d}t} = B_1[\mathrm{Na(1)}] - B_2[\mathrm{Na(2)}] \tag{14}$$

where

$$A_g = k_1[e^-] + k_6[M]$$
$$A_1 = k_2[e^-] + k_3[e^-] + k_5[M] + k_8[M] - k_9$$
$$A_2 = k_4[e^-] + k_7[M] \qquad B_1 = k_3[e^-] + k_8[M]$$
$$B_2 = k_4[e^-] + k_7[M] + k_{10}$$

and the [ ] brackets denote concentrations and

$$[\mathrm{Na}(g)] + [\mathrm{Na(1)}] + [\mathrm{Na(2)}] = [\mathrm{Na}] \tag{15}$$

due to conservation. Using the total sodium (Na) number density, from the DSMC solution, the sodium number densities of the ground and excited states can be obtained by solving Eqs. (13–15) for the quasi-steady-state limit: that is, the derivatives of the excited-state concentrations are assumed to be zero. If there were sufficient collisions such that the system was in a fully equilibrium state, the number of atoms in the ground and excited states would satisfy a Boltzmann distribution:

$$\frac{N_i}{N} = \frac{g_i e^{-E_i/kT}}{Q} \tag{16}$$

where

$$Q = \sum_{i=0}^{n} g_i e^{-E_i/kT} \tag{17}$$

and the subscript i refers to the ground or excited state, g_i is the degeneracy of electronic state i, E_i is the energy level of the excited state, and N_i is the number density of the sodium ith energy level and

$$N = \sum_i N_i \tag{18}$$

The results discussed in Sec. IV will show that a Boltzmann distribution does not hold.

The radiation obtained with the QSS and Boltzmann distributions will be compared in Sec. IV. The radiation intensity from an excited state to the ground state along a line-of-sight (LOS) observation from the vehicle surface s to the observer is

$$\Delta I_\lambda = \int_s^\infty \frac{N_i}{\tau} \cdot \frac{hc}{\lambda} \cdot \frac{1}{\phi_\lambda} \cdot \frac{\mathrm{d}x}{4\pi} \tag{19}$$

where ϕ_λ is the instrument Doppler shape function, and s represents the reentry vehicle surface. The radiation energy flux to the instrument collecting optics is the integration over all observed LOS lines, multiplied by the solid angle between observer and target, as

$$I_\lambda = \frac{1}{d^2} \int_{A_s} \Delta I_\lambda \, \mathrm{d}A \tag{20}$$

where A_s is the surface radiation area, and d is the distance between the observer and the target. Only radiation from the forebody surface is considered and the solid angle is assumed to be the same for all forebody surface elements.

III. Contribution of Potential Sodium-Ionization Processes

If sodium were ionized by electron and neutral particles in the high-temperature shock region, the atomic-sodium number density in both the ground and excited states would decrease. Since sodium and its ion have significantly different optical emissions, it is necessary to estimate the electron- and neutral-impact sodium-ionization probabilities in order to evaluate the importance of sodium impact ionization processes.

The ionization reaction probability is generally defined as the ratio of the ionization cross section to the total collision cross section. Walters [19] estimated electron-sodium total collision cross sections using a two-channel nonadiabatic model solving the coupled Schröodinger equation and obtained a good agreement with the experimental data of Kasdan et al. [20]. The calculation and experimental results showed that electron-sodium total collision cross sections are about 100 to 200 Å^2 in the energy range of 1 to 5 eV. Hayhurst and Telford [21] used a quadrupole mass spectrometer to determine sodium-ionization rates in low-temperature-flame environments and found that the atomic-sodium electron-impact-ionization activation energy is about 4.96 eV. Tan et al. [16] summarized the experimental results of the total-sodium-electron ionization cross sections and showed that the ionization cross section is approximately 0.1 Å^2 for a collision energy of 5.0 eV. From these sources, it may be concluded that the sodium-ionization probability by electron impact is less than 0.1% for the small fraction of high-energy electrons present in the tail of the Maxwellian distribution for the reentry cases studied in this work.

Since there are limited data on neutral-impact sodium total and ionization collision cross sections, Drawin [22] proposed a semi-empirical approach to estimate atom–atom ionization cross sections based on the corresponding electron–atom ionization cross section. Drawin estimated the ionization cross section of a target atom, $\sigma_e(E)$, by an incident electron to be

$$\sigma_e(E) = N_b 4\pi a_0^2 \left(\frac{Ry}{U}\right)^2 \frac{u-1}{u^2} \tag{21}$$

where $u = E/U$, E is the impact energy, U is the ionization potential of the target atom, a_0 is the Bohr radius, Ry is the Rydberg energy of 13.6 eV, and N_b is the number of the outer-shell electrons in the target atom. Figure 2 shows the electron-impact sodium-ionization cross section using Eq. (21), which is in reasonable agreement with the experimental data shown in the work of Tan et al. [16]. For the atom–atom ionization collision cross section, Drawin [22] suggested that the parameter u in Eq. (21) be replaced by

$$u = 1 + \frac{2m_e}{m_a + m_e}(W - 1) \tag{22}$$

where m_e and m_a are the electron and atomic mass, and

$$W = \frac{E - U}{U} \tag{23}$$

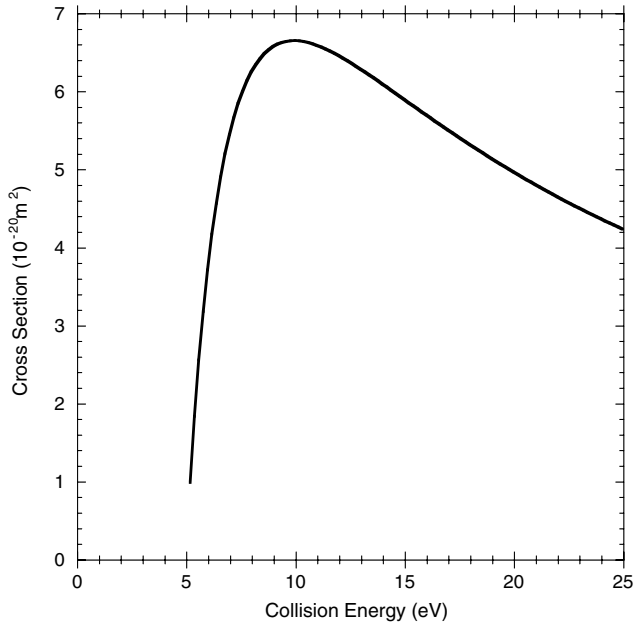

Fig. 2 Electron-impact sodium-ionization cross section estimated by the Drawin's [22] semi-empirical approach.

Drawin [22] also introduced the ratio of the atomic mass to hydrogen atom mass to estimate the atom–atom ionization cross section as

$$\sigma_a(E) = N_b^2 4\pi a_0^2 \left(\frac{Ry}{U}\right)^2 \frac{m_a}{m_H}\frac{2m_e}{m_a + m_e}\xi \tag{24}$$

where

$$\xi = (W-1)\Big/\left(1 + \frac{2m_e}{m_a + m_e}(W-1)\right)^2$$

It can be seen from Eqs. (22–24) that the atom–atom-ionization activation energy is two times greater than the electron-impact-ionization activation energy. Therefore, the atom-impact sodium-ionization activation energy is about 10 eV. Figure 3 shows the atom-impact sodium-ionization cross section obtained from Eq. (24). It was concluded by Kunc and Soon [23] that Eq. (24) is a good representation of the atom-impact sodium-ionization cross section. Kresin and Scheidemann [24] used a molecular beam-scattering technique to measure the atom–alkali *total* collision cross sections and found that the atom–potassium total collision cross section is more than 700 Å^2, which is consistent with other available data. Therefore, the reaction probability of atom-impact sodium ionization is smaller than that of electron-impact sodium ionization.

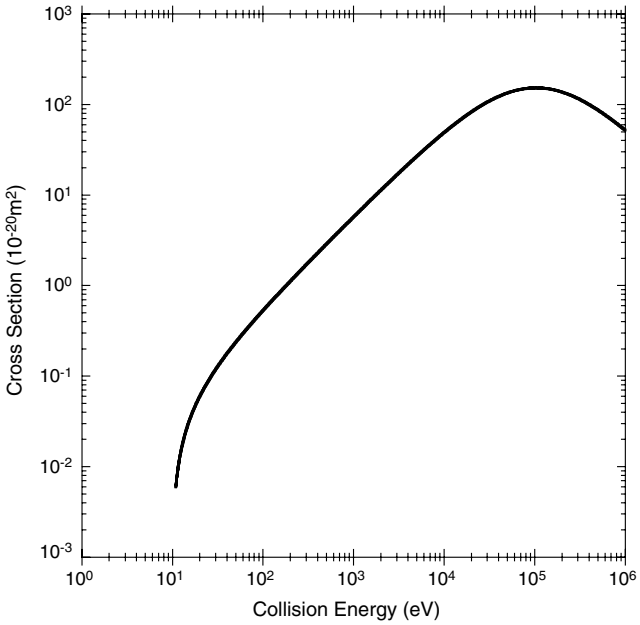

Fig. 3 Atom-impact sodium-ionization cross section estimated by the Drawin's [22] semi-empirical approach.

Based on the above analysis of the electron- and atom-impact sodium-ionization reaction activation energies and reaction probabilities, it was found that sodium-ionization processes are negligible for the Mach number regime and blunt- and slender-body reentry cases studied in this work. For these reasons, the sodium-ionization processes are not modeled in the DSMC flow simulations.

IV. DSMC and QSS Simulation Results

The DSMC based SMILE software [25] is used in this work to model the 2-D axisymmetric blunt-body Stardust sodium-ablation calculations, as well as a 10 deg half-angle-cone slender body with a length of 1.0 m at high altitudes. The freestream and surface conditions as well as DSMC computational parameters are summarized in Table 2. A cell adaption technique is used to automatically divide cells into smaller subcells so that the flow mean free path is approximately on the same order as the local cell size. The Stardust and slender-body forebody stagnation points are located at the origin of the coordinate system. The air-species chemical and ionization reactions were summarized in [6]. Note that any potential reactions of the ablated sodium with the air-derived flowfield species are neglected in the DSMC modeling. The assumption is that although such collisions may affect the sodium excited-state population, they are too few to affect the gas dynamics [10].

In order to test the implementation technique of modeling sodium ablation from a hypersonic body surface, such as Stardust, numerical comparisons were performed between two DSMC codes, SMILE and Monaco [9]. It was shown in [9] that good agreement of sodium number density, velocities and temperatures along the Stardust forebody stagnation streamline with a surface ablation rate of $3.5 \times 10^{19}/(\text{m}^2 \cdot \text{s})$ into a vacuum environment was obtained between the two DSMC codes. In addition, in SMILE, two numerical techniques, full-spherical sources and half-spherical sources, both placed in cells adjacent to the wall, were used and tested to model sodium ablation from surface. With adequate grid resolution, either of these two SMILE techniques will work because the full spherical source particles move towards and collide essentially immediately with the wall. Since the wall is assumed to be fully thermally accommodated and diffuse, the reflected particles are expected to behave exactly the same as the half-spherical source molecules moving towards the upstream. The simulation results of sodium ablation and excitation in the Stardust-reentry flow are discussed below.

Numerical studies of the Stardust thermal protection system PICA ablation [9] indicate that the total mass flux of material blowing off the surface at this flow condition is 1.26×10^{-12} kg/(m$^2 \cdot$ s). Because of the material impurity, the mass fraction of sodium in the ablative material is about 4.0×10^{-5}, corresponding to a surface flux

Table 2 Freestream and surface parameters

Parameter	Stardust	Slender
Freestream temperature, K	217.6	185.0
Freestream number density, molecules/m^3	2.6388×10^{20}	4.18×10^{20}
Freestream velocity, m/s	12,391.8	7500.
Freestream O_2 mole fraction, %	23.67	21.0
Freestream N_2 mole fraction, %	76.23	79.0
Surface temperature, K	2000	1000
Surface sodium-ablation rate, molecules/(m$^2 \cdot$ s)	1.43×10^{19}	1.43×10^{19}
DSMC computational domain axial direction, m	$-0.15, -3.05$	$-1.0, -4.0$
Radial direction, m	$0, -0.8$	$0, -1.0$
Cell size, m	1.5×10^{-3}	5.0×10^{-3}

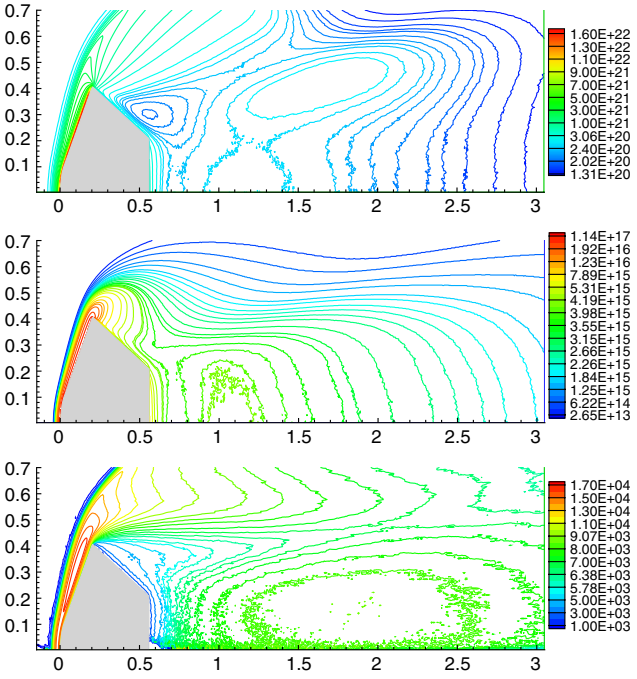

Fig. 4 Contour distributions of Stardust flow total number density per m^3 (top), sodium number density per m^3 (middle), and translational temperature in Kelvin. The axial and radial dimensions are in meters.

of 1.43×10^{19} atoms/(m$^2 \cdot$ s). The DSMC solutions of total, sodium, and flow temperatures are shown in Fig. 4. Using the species number densities from the DSMC simulation, the sodium number densities in the ground and excited states can be obtained by solving the linear set of Eqs. (13–15) at the steady-state condition. The number-density contours of the sodium ground and excited $^2P_{3/2,1/2}$ and $^2D_{5/2}$ states obtained from the QSS solutions are shown in Fig. 5. It can be seen that the number density of the ground-state sodium atom is about 2 to 3 orders of magnitude greater than that of the $^2P_{1/2}$ excited state, and the $^2P_{1/2}$ excited-state sodium atom is about 2

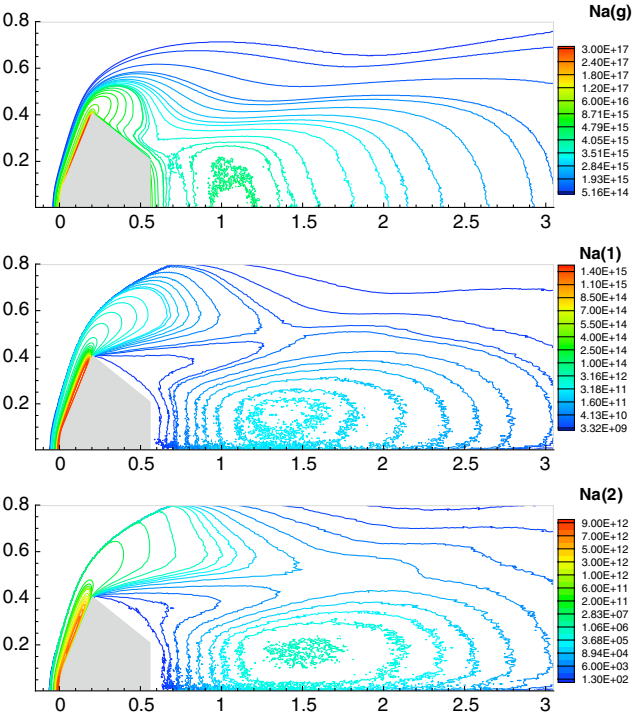

Fig. 5 Number-density contours of sodium in ground and excited states for Stardust reentry at 81 km.

orders of magnitude greater than the $^2D_{5/2}$ excited state. The quantitative results of the sodium number densities ground and excited states along the forebody and afterbody stagnation lines are shown in Fig. 6. It can be seen from Fig. 6 that sodium number density decreases rapidly in the forebody region for flow locations upstream of the body since the ablated sodium diffusion direction is opposite to the flow direction. However, sodium number density along the afterbody stagnation line is almost constant since the sodium diffusion direction is the same as the expanding flow. This result is consistent with the observed Stardust-reentry long wake trail.

To evaluate the degree of nonequilibrium sodium radiation, Fig. 7 compares the sodium number-density ratio of QSS to Boltzmann solutions for the excited states along the forebody and afterbody stagnation lines. It can be seen that in the forebody region the QSS solution of the sodium number density for the $^2P_{1/2}$ excited state is about 10% of the equilibrium Boltzmann solution, while in the afterbody region the ratio of QSS and Boltzmann solutions is about 10^{-4}. Therefore, a larger degree of nonequilibrium radiation exists in the afterbody region than the forebody region since the temperature and collision rate in the afterbody region is low, requiring longer times to reach equilibrium.

The sodium radiation intensity can be calculated from the QSS solution based on Eq. (20). It is assumed that radiation from Stardust forebody surface region is the main contribution to the measured radiation energy flux. According to [5], the observation distance d of Stardust forebody radiation intensity at 81 km is about 400 km, and the width of the instrument Doppler shape function ϕ_λ is about

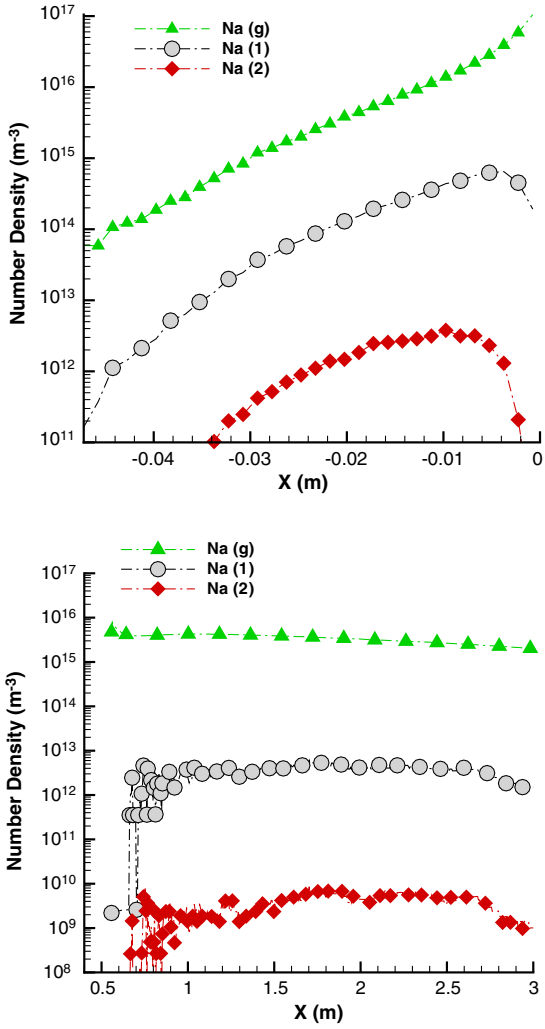

Fig. 6 Distributions of sodium number density per m^3 at ground and excited states along forebody (top) and afterbody (bottom) stagnation lines. The axial and radial dimensions are in meters.

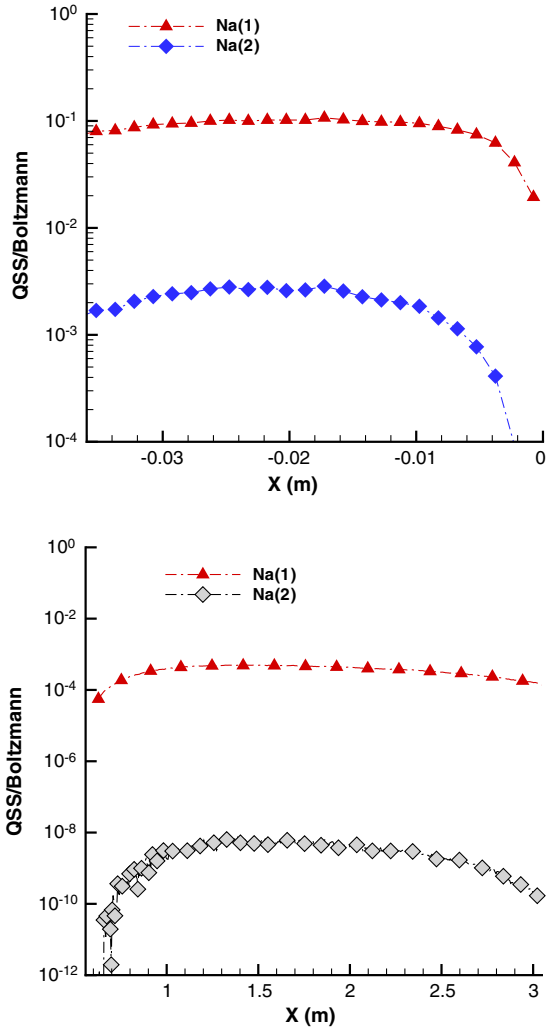

Fig. 7 Sodium number-density ratio of QSS to Boltzmann solutions in excited states along forebody (top) and afterbody (bottom) stagnation lines.

0.416 nm. The integrated sodium-radiative intensity over the forebody surface at $^2P_{3/2,1/2}$ centered at at 589 nm is about 2.30×10^{-10} W/(m$^2\cdot$nm), which is quite close to the measured value of 4.50×10^{-10} W/(m$^2\cdot$nm) as shown in Fig. 1. The difference between the calculated and measured intensity may be due to the effects of gaseous absorption and observation window transparency, and some uncertainties of sodium-excitation rates and sodium surface ablation rate used in the DSMC calculation. It may be concluded that Stardust-reentry sodium radiation intensity at 81 km is reasonably predicted by the quasi-steady-state method.

The high-speed blunt-body Stardust-reentry flow is characterized by intensive chemical reactions and ionizations in the detached high-temperature bow-shock region. However, for a slender-body reentry flow, there typically exists a rather weak attached oblique shock. The sodium radiation flow may have different features in the slender-body entry flow from the blunt-body flow, due to different flow features. Therefore, it is necessary to further study sodium radiation behavior in a slender-body reentry flow. A detailed study of blunt- and slender-body reentry flow can be found in [8]. Here, we choose a 10 deg half-angle-cone slender body with a length of 1.0 m at an altitude of 80 km, the freestream velocity is 7.0 km/s, and the surface sodium-ablation rate is chosen to be the same as the blunt-body surface ablation rate.

Figure 8 shows the slender-body flow total number density (top), sodium number density (middle), and translational temperature contours, and the distributions of these parameters along the wake centerline are shown in the top of Fig. 9. Ionization reactions were not considered, since the oblique shock generates temperatures even lower than for a blunt body, for which electron-impact sodium excitation was found not to be important. As shown in the bottom of Fig. 9, the excited sodium number density at $^2P_{1/2}$ state generated by molecular-impact sodium excitation is more than six orders of magnitude less than the ground-state sodium number density in the wake region, and the excited sodium number density at $^2D_{5/2,3/2}$ state is almost neglectable. Although the ground-state sodium number densities are around 10^{16} to 10^{15} molecules/m^3 in both the blunt- and slender-body wake regions, the excited-state sodium number density in the slender-body wake region is more than four orders of magnitude less than the value in the blunt-body wake region. This is because the excited sodium in the highly concentrated blunt forebody region is able to diffuse to the afterbody wake region. Therefore, it

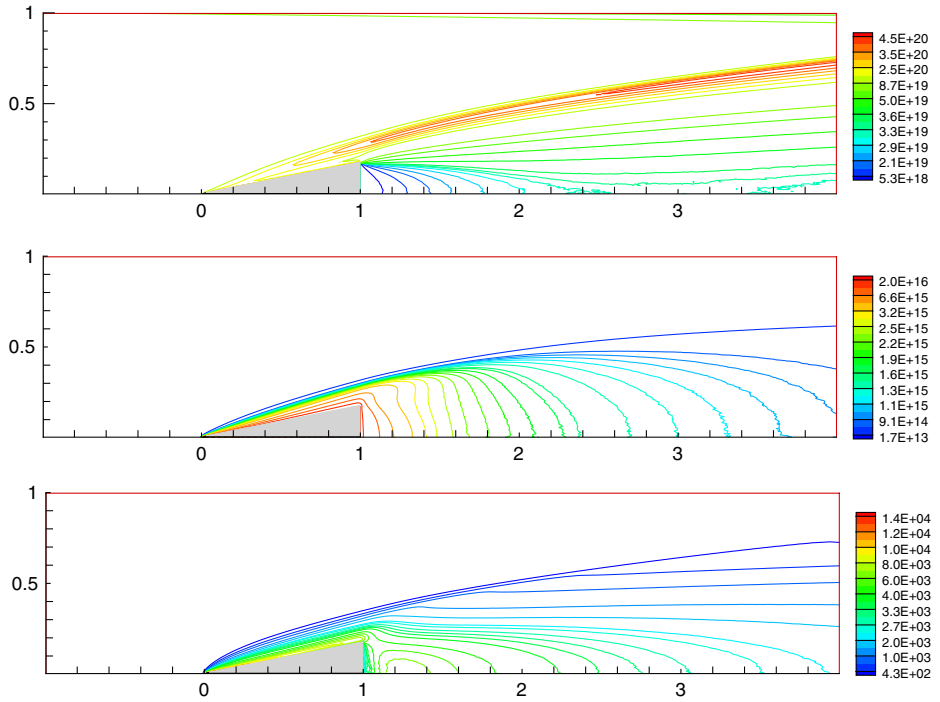

Fig. 8 Contour distributions of slender-body flow total number density per m^3 (top), sodium number density per m^3 (middle), and translational temperature in Kelvin. The axial and radial dimensions are in meters.

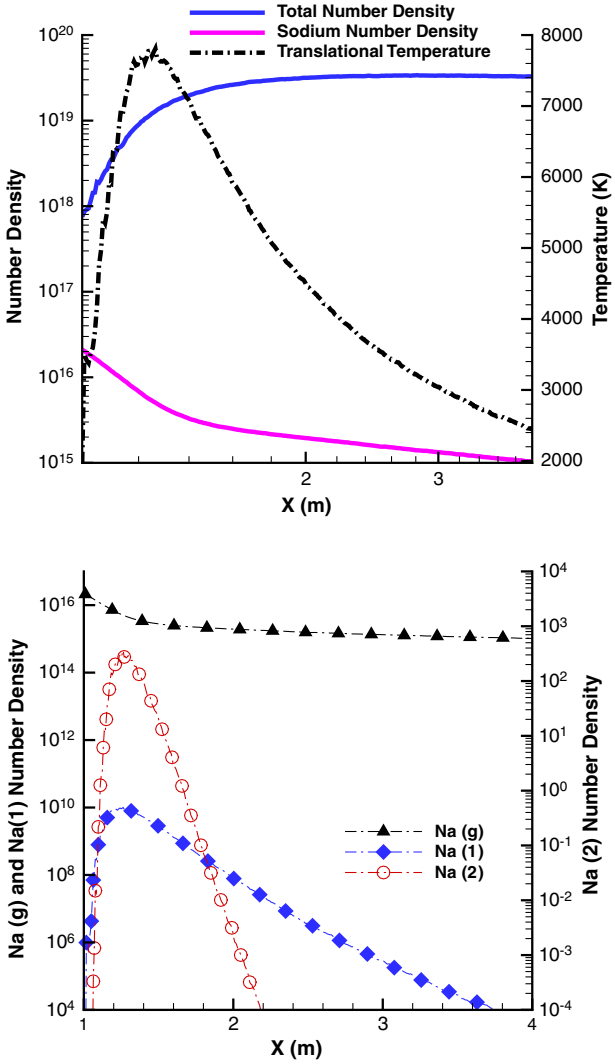

Fig. 9 Total number density, sodium number density, and translational temperature along the slender wake centerline (top) and sodium number-density distributions in the ground and excited states along the wake centerline (bottom).

may be concluded that sodium radiation in the slender-body entry flow may be observed; however, the radiation intensity will be orders of magnitude less than the value observed in the blunt-body entry flow.

V. Conclusions

The particle-based direct simulation Monte Carlo (DSMC) method was used to obtain blunt- and slender-body reentry flow solutions, and a quasi-steady-state (QSS) model was developed to calculate the sodium number-density distributions for ground and excited states. This work shows that the calculated sodium radiation intensity, based on the developed QSS model, agrees reasonably well with the observed data for the Stardust-reentry case. The good agreement between modeling and experiment suggests that the flow modeling predicts the correct electron temperature and electron number density. It also suggests that the QSS model may be applied to different geometries for similar freestream conditions.

For the blunt-body reentry flow, the electrons created from the ionization reactions in the bow-shock region have a strong impact on the sodium-excitation process. However, there are no electrons in the slender-body reentry flow due to the weak oblique shock, and only neutral species contribute to the sodium-excitation process. Therefore, the sodium radiation intensity in a slender-body reentry flow is orders of magnitude less than in a blunt-body reentry flow for the same sodium surface ablation rate. It was also found that electron- and neutral-impact sodium-ionization reactions have high reaction activation energy and low reaction probabilities. Therefore, the impact of sodium ionization has a negligible impact on its excitation process for both slender and blunt cases studied in this work.

Acknowledgments

The research performed at Pennsylvania State University is supported by NASA through grant no. NNX07AC47A. Special thanks to M. Ivanov of the Institute of Theoretical and Applied Mechanics for the use of the original SMILE code.

References

[1] Dong, S., Ma, Y., and Tan, H., "Modeling of High-Temperature Air Species Nonequilibrium Spectral Radiation Properties," *Journal of Thermophysics and Heat Transfer*, Vol. 22, No. 2, 2008, pp. 301–305. doi:10.2514/1.33547

[2] Wray, A. A., Ripoll, J. F., and Prabhu, D., "Computation of Radiation in the Apollo AS-510 Reentry Using Opacity Distribution Functions," *AIAA Journal*, Vol. 45, No. 9, 2007, pp. 2359–2363. doi:10.2514/1.28520

[3] Harvey, G. A., "Photometric Analysis of Spectrograms of Two Trailblazer Payload Reentry," NASA TN D-3389, Hampton, VA, Apr. 1996.

[4] Lenard, M., "Ionization of Cesium and Sodium Contaminated Air in the Hypersonic Slender Body Boundary Layer," Space Sciences Laboratory, Missile and Space Division, No. R64SD22, Aug. 1964.

[5] Jenniskens, P., "Observations of the Stardust Sample Return Capsule Entry with a Slitless Echelle Spectrograph," 46th Aerospace Sciences Meeting, AIAA Paper 2008-1214, Reno, NV, 2008.

[6] Ozawa, T., Zhong, J., and Levin, D., "Development of Kinetic-Based Energy Exchange Models for Noncontinuum Ionized Hypersonic Flows," *Physics of Fluids*, Vol. 20, No. 4, 2008, Paper 046102.

[7] Zhong, J., Ozawa, T., and Levin, D. A., "Modeling of Stardust Ablation Flows in the Near-Continuum Flight Regime," *AIAA Journal*, Vol. 46, No. 10, Oct. 2008, pp. 2568–2581. doi:10.2514/1.36196

[8] Zhong, J., Ozawa, T., and Levin, D. A., "Comparison of High-Altitude Hypersonic Wake Flows of Slender and Blunt Bodies," *AIAA Journal*, Vol. 46, No. 1, 2008, pp. 251–262. doi:10.2514/1.31056

[9] Boyd, I. D., Zhong, J., Levin, D. A., and Jenniskens, P., "Flow and Radiation Analyses for Stardust Entry at High Altitude," 46th Aerospace Sciences Meeting, AIAA Paper 2008-1215, Reno, NV, 2008.

[10] Levin, D., Candler, G., and Collins, R., "An Overlay Method for Calculating Excited State Species Properties in Hypersonic Flows," *AIAA Journal*, Vol. 35, No. 2, Feb. 1997, p. 288. doi:10.2514/2.90

[11] Zecca, A., Karwasz, G. P., and Brusa, R. S., "One Century of Experiments on Electron-Atom and Molecule Scattering: A Critical Review of Integral Cross Sections," *Rivista del Nuovo Cimento*, Vol. 19, No. 3, 1996, pp. 1–146. doi:10.1007/BF02742990

[12] Rautian, S. G., and Yatsenko, A. S., "Grotrian Diagrams," *Physics-Uspekhi*, Vol. 42, No. 2, 1999, pp. 205–208. doi:10.1070/PU1999v042n02ABEH000519

[13] Zaslonko, I. S., and Kogarko, S. M., "Excitation of Sodium in Certain Reactions Behind Shock Waves," *Combustion, Explosion and Shock Waves*, Vol. 6, No. 2, pp. 175–182. doi:10.1007/BF00742925

[14] Stone, P. M., and Kim, Y., "Electron-Impact Cross Sections for Ground State to NP Excitations of Sodium and Potassium," *Journal of Research of the National Institute of Standards and Technology*, Vol. 109, No. 5, 2004, pp. 505–515.

[15] Fujii, K., and Srivastava, S. K., "A Measurement of the Electron-Impact Ionization Cross Section of Sodium," *Journal of Physics B: Atomic, Molecular and Optical Physics*, Vol. 28, No. ??, 1995, pp. L595–L563.

[16] Tan, W. S., Shi, Z., Yang, C. H., and Vuskovic, L., "Electron-Impact Ionization of Laser-Excited Sodium Atom," *Physical Review A*, Vol. 54, No. 5, Nov. 1996, pp. 3710–3713. doi:10.1103/PhysRevA.54.R3710

[17] Hertel, I. V., Hofmann, H., and Rost, K. A., "Electronic to Vibrational-Rotational Energy Transfer in Collisions of Na with SIMPLE Molecules," *Chemical Physics Letters*, Vol. 47, No. 1, Apr. 1977, pp. 163–167. doi:10.1016/0009-2614(77)85330-X

[18] Bird, G. A., *Molecular Gas Dynamics and the Direct Simulation of Gas Flows*, Oxford Science, Oxford, 1994, p. 458.
[19] Walters, H. R. J., "On the Elastic Scattering of Electrons by Lithium and the Total Cross Sections for Electron Impact on Lithium, Sodium and Potassium," *Journal of Physics B: Atomic and Molecular Physics*, Vol. 9, No. 2, 1976, pp. 227–237. doi:10.1088/0022-3700/9/2/011
[20] Kasdan, A., Miller, T. M., and Bederson, B., "Absolute Measurements of Total Cross Sections for Electron Scattering by Sodium Atoms," *Physical Review A*, Vol. 8, 1973, pp. 1562–1569. doi:10.1103/PhysRevA.8.1562
[21] Hayhurst, A. N., and Telford, N. R., "Kinetics of Thermal Ionization of Alkali Metals in Flams," *Journal of the Chemical Society. Faraday Translations I*, Vol. 68, 1972, pp. 237–248. doi:10.1039/f19726800237
[22] Drawin, H. W., "Influence of Atom-Atom Collisions on the Collisional-Radiative Ionization and Recombination Coefficients of Hydrogen Plasmas," *Zeitschrift für Physik*, Vol. 225, 1969, pp. 483–493. doi:10.1007/BF01392775
[23] Kunc, J. A., and Soon, W. H., "Analytical Ionization Cross Sections for Atomic Collisions," *Journal of Chemical Physics*, Vol. 95, No. 8, 1991, pp. 5738–5751. doi:10.1063/1.461622
[24] Kresin, V. V., and Scheidemann, A., "Scattering of Neutral Metal Clusters: Long-Range Interactions and Response Properties," *Journal of Chemical Physics*, Vol. 98, No. 9, 1993, pp. 6982–6988. doi:10.1063/1.464740
[25] Ivanov, M. S., Markelov, G. N., and Gimelshein, S. F., "Statistical Simulation of Reactive Rarefied Flows: Numerical Approach and Application," AIAA Paper 98-2669, June 1998.

D. Kontinos
Guest Editor